Monomer Composition as a Mechanism to Control the Self-Assembly of Diblock Oligomeric Peptide-Polymer Amphiphiles.

Benjamin P. Allen^[a], Sabila K. Pinky^[b], Emily E. Beard^[a], Abigail A. Gringeri^[a], Nicholas Calzadilla^[a], Matthew A. Sanders^[a], Yaroslava G. Yingling^{*[b]}, and Abigail S. Knight^{*[a]}

[a] Department of Chemistry, The University of North Carolina at Chapel Hill, Chapel Hill, North Carolina 27599, United States [b] Department of Materials Science and Engineering North Carolina State University Raleigh, North Carolina 27695. United States

KEYWORDS biomimetic, nanoparticles, peptide-polymer amphiphile, polymer chemistry, self-assembly

ABSTRACT: Diblock oligomeric peptide-polymer amphiphiles (PPAs) are biohybrid materials that offer versatile functionality by integrating the sequence-dependent properties of peptides with the synthetic versatility of polymers. Despite their potential as biocompatible materials, the rational design of PPAs for assembly into multi-chain nanoparticles remains challenging due to the complex intra- and intermolecular interactions emanating from the polymer and peptide segments. To systematically explore the impact of monomer architecture on nanoparticle assembly, PPAs were synthesized with a random coil peptide (XTEN2) and oligomeric alkyl acrylates with unique side chains: ethyl, tert-butyl, n-butyl, and cyclohexyl. Experimental characterization using electron and atomic force microscopies demonstrated that tail hydrophobicity impacted accessible morphologies. Moreover, characterization of different assembly protocols (i.e., bath sonication and thermal annealing) revealed that certain tail compositions provide access to kinetically trapped assemblies. All-atom molecular dynamics simulations of micelle structure formation unveiled key interactions and differences in hydration states, dictating PPA assembly behavior. These findings highlight the complexity of PPA assembly dynamics and serve as valuable benchmarks to guide the design of PPAs for a variety of applications including catalysis, mineralization, targeted sequestration, antimicrobial activity, and cargo transportation.

Introduction

Multi-chain nanoparticles are instrumental in nanotechnology and nanomedicine,1,2 serving as versatile chemosensors3 and with applications in organic semiconductors4,5 and biomineralization.^{6,7} Despite their wide-ranging applications, their rational design remains challenging due to the complex network of inter- and intramolecular interactions formed between macromolecules. Many nanoparticles are assembled through the phase separation of hydrophobic and hydrophilic blocks in aqueous solution. While hydrophobic interactions predominantly drive this self-assembly, the assembled morphologies are further influenced by a concert of non-covalent interactions (e.g., electrostatics, van der Waals, π-π stacking, and hydrogen bonding) and processing steps such as the assembly technique and filtration.^{2,7-9} This interplay of variables provides tunability of both nanoparticle morphology and size, consequently dictating the functionality of the assembled structure. Therefore, understanding the interplay of these interactions is paramount in the rational design of functional nanoparti-

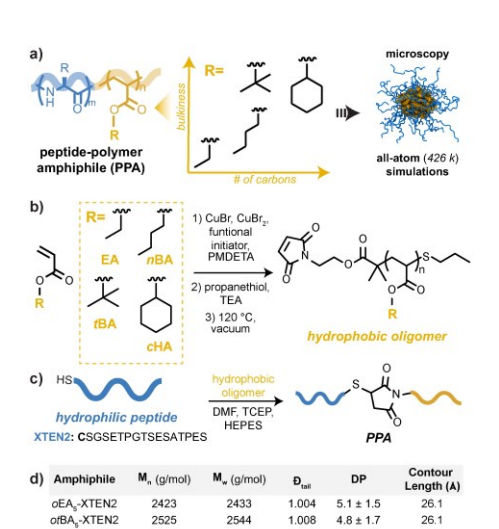
Peptide amphiphiles (PAs) uniquely incorporate proteinlike functions into assembled nanostructures when coupled to a hydrophobic tail.^{1,7,10,12,13} Assembled PAs can template biomineralization of inorganic nanoparticles,¹¹ induce phosphorylation for therapeutics,¹² and outperform the function of their native protein analogs^{13,14}. While altering the hydrophobic block composition using aromatic moieties, amino acids, and/or multi-chain lipid-like tails modulates the assembled morphology, these moieties have a narrow scope of easily accessible hydrophobic tails which limits the range of accessible morphologies and assembly dynamics

Diblock peptide-polymer amphiphiles (PPAs) are biohybrid materials that combine sequence-defined peptides with oligomeric tails synthesized with common polymerization techniques.15-17 Monomer selection, molecular weight, and dispersity enable tunability of the hydrophobic amphiphile component, which in turn dictates the final assembled morphology. 18-20 We have previously demonstrated that oligomeric diblock PPAs composed of oligo(ethyl acrylate) tails and random-coil peptides exhibit similarities to block copolymers, assembling into nanoparticles with diverse morphological distributions influenced by the average molecular weight and dispersity of the hydrophobic oligomer.²¹ Efforts with amphiphilic block copolymers have demonstrated that the chemical composition of monomers can impact both the packing density8,22 and exchange dynamics^{8,23,24} of multi-chain assemblies. Though the impact of polymer composition (as described by glass transition temperature) on PPA nanoparticle stability has been studied, its utility in augmenting PPA morphology and assembly dynamics has remained unexplored.16

Herein, we investigate the self-assembly of PPAs composed of a random coil peptide and acrylate oligomers with variable monomer chemistry (ethyl, tert-butyl, n-butyl, and cyclohexyl) using a combination of experimental techniques to probe the morphological distributions and computational methods to provide mechanistic insights. Through experimental characterization by electron and atomic force microscopies, we analyze how both the oligomeric tail hydrophobicity and assembly mechanism impact nanoparticle sizes and morphologies. Additionally, all-atomistic molecular dynamic simulations of the micelle structure of three selected amphiphile assemblies reveal the influence of intramolecular interactions and presence of core hydration, enabling deeper mechanistic insights. This integrated approach highlights the tunability afforded by the hydrophobic component of the PPA, yielding morphological distributions that can be modulated using both hydrophobicity and the assembly mechanism.

Results and Discussion

To investigate how the morphology and dynamics of nanoparticles formed by diblock peptide-polymer amphiphiles (PPA) can be tuned via the hydrophobic oligomeric tail, four alkyl acrylate oligomers were synthesized with consistent degrees of polymerization (DPtail) but variable pendent chain composition: oligo(ethyl acrylate) (oEA), oligo(tertbutyl acrylate) (otBA), oligo(n-butyl acrylate) (onBA), and oligo(cyclohexyl acrylate) (ocHA) (Figure 1a). The oligomers were synthesized using atom transfer radical polymerization. A protected maleimide initiator was used to facilitate both coupling to a cysteine-containing peptide and access to short oligomers with controlled molecular weight dispersity (Figures S1-S2).25 Post polymerization, the oligomers were substituted with propanethiol, removing the bromine chain end to prevent off-target reactions. The maleimide chain end was then deprotected under vacuum and heated to generate a reactive handle for peptide coupling (Figures 1b and S3-S18).21 To limit the impact of peptide secondary structure and incorporate a hydrophilic block capable of solubilizing the series of hydrophobic oligomers, we chose the charged random coil peptide XTEN2 containing 17 amino acids (Figures 1c and S19).26,27 XTEN2 was synthesized using solid phase peptide synthesis, incorporating an N-terminal cysteine residue to couple the peptide with the deprotected maleimide terminus of each of the hydrophobic oligomers. Following purification of the peptide using reversed-phase high performance liquid chromatography (HPLC), the thiol-maleimide coupling was facilitated by 4-(2-hydroxyethyl)-1-piperazineethanesulfonic acid (HEPES, 20x) and tris(2-carboxylethyl)phosphine (TCEP, 2x) in DMF at 85 °C. Purification of the amphiphiles was accomplished by precipitating the crude mixture in 1:1 cold diethyl ether/hexanes followed by using disposable reversed-phase columns to remove unreacted peptide and polymer from the amphiphile with acetonitrile gradients and/or tetrahydrofuran (THF). Solvent gradients were used to control the average degree of polymerization (DPtail) of the PPA, targeting an average length of 5 monomer units for each PPA (Scheme S1). After purification, characterization via liquid chromatography-mass spectrometry (LC-MS) enabled calculation of the DPtail, number average molecular weight (M_n), and weight average molecular weight (M_w) of



2543

1.005

 4.8 ± 1.5

onBA.-XTEN2

ocHA,-XTEN2

2528

Figure 1. Overview of oligomeric diblock peptide-polymer amphiphile (PPA) design and synthesis. (a) Schematic illustrating PPA design containing a series of hydrophobic tails varying the monomer bulkiness and/or carbon number of the pendent moiety and complementary experimental and computational characterization. (b) Alkyl acrylate oligomers were synthesized with a functional initiator containing a protected maleimide and atom transfer radical polymerization with ethyl acrylate (EA). n-butyl acrylate (nBA), tert-butyl acrylate (tBA), or cy clohexyl acrylate (cHA). Polymerizations were performed in acetone at 50 °C (monomer 25 eq, acetone 50% v/v, functional initiator 1 eq, CuBr 0.5 eq, Cu(II)Br₂ 0.025 eq, N,N,N',N"-pentamethyldiethylenetriamine (PMDETA) 0.53 eq) and quenched prior to full conversion. Subsequent thiol substitution of the bromine chain (10 eq propanethiol, 11 eq triethylamine (TEA), rt, on) and deprotection (120 °C, 2h) formed oligomers with terminal maleimides. (c) The XTEN2 peptide was coupled to the maleimide using an N-terminal cysteine residue using 4-(2hydroxyethyl)-1-piperazineethanesulfonic acid (HEPES, 20x) and tris(2-carboxylethyl)phosphine (TCEP, 2x) in DMF (85 °C, 5h). (d) The number average molecular weight (Mn), weight average molecular weight (M_w), molecular weight dispersity (Đ), and average degree of polymerization (DPtail) for each PPA oligomer tail calculated by integrating chromatograms obtained from integrated LC chromatographs. Contour length (Å) was calculated for each PPA using Discovery Studio Visualizer

each amphiphile (Figures 1d and S20-S27). The PPA series had low dispersity values ($\theta\approx 1$) as calculated based on both integrated absorbance and total ion chromatograms (Figure 1d, S24-27). To provide an alternative measure of the dispersity of amphiphile lengths in each PPA mixture, we calculated the standard deviation for each PPA distribution. The values reported in Figure 1 are calculated from the absorbance chromatogram, as we anticipate that the additional alkyl moieties will have a limited impact on the absorbance coefficient, whereas the ionization could be more significantly impacted. 28 The purified series of PPAs contain an average tail length of 5 monomer units with similar

ranges of monomer lengths present. Additionally, simulations of discrete oligomeric tails (DP $_{\text{tail}} = 5$) visualized using Discovery Studio Visualizer revealed comparable contour lengths (Figure 1d), further supporting that differences in nanoparticle properties amongst the PPA assemblies will primarily be driven by the monomer composition.

To evaluate the impact of tail composition on the accessible assembled morphologies, each amphiphile (1 mM) was assembled in HEPES buffer (50 mM, pH 7) via bath sonication (1 h).21 The assemblies were visualized via negativelystained transmission electron microscopy (NS-TEM) (Figures 2a and S28-S31), showing a mixture of spherical particles and supramolecular assemblies of cylinders. Cryogenic electron microscopy (cryo-EM) of the four PPA assemblies confirmed spherical particles to be mixtures of micelles (commonly found in clusters similar to other block copolymer) and larger nanostructures that display less contrasted cores (Figure 2b). Though we were able to verify the presence of a defined membrane indicating vesicle formation in oEA5-XTEN2, we did not observe the characteristic outer ring for other three PPAs. This phenomena has been seen previously with PEO-b-PEA copolymers of similar size scale (4-20 nm), forming hollow nanoparticles without well-defined bilayers as characterized using cryo-EM.29 We hypothesize that a bilayer is challenging to observe due to the small size scale of these particles, but will refer to these as vesiclelike assemblies or nanoparticles to encompass other bilayer-containing morphologies (e.g., semi-vesicles or quasivesicles) 19,30-32 Cylindrical bundles were challenging to observe via cryo-EM; thus, we further characterized the assembled morphologies using in-solution atomic force microscopy (AFM; Figures 2c and S32-S35) to confirm the bundles are present in solution. AFM confirmed the presence of spherical particles in all PPA assemblies and supramolecular assemblies of cylinders in onBA5-XTEN2 and ocHA5-XTEN2. In contrast to our previous study, oEA5-XTEN2 did not form cylindrical structures, but the distributions of micelles and vesicle-like particles remained consistent²¹. We hypothesize that cylindrical structures are challenging to maintain for these PPAs lacking significant intermolecular hydrogen bonding, and thus that small changes to the distribution impact their accessibility. While the cylindrical bundles formed by onBA5-XTEN2 and ocHA5-XTEN2 exhibit well-defined bundles (average diameter = 23 ± 2 nm; Figure S34), ocHA5-XTEN2 forms larger heterogenous assemblies (Figure S35). We also note that these bundles are present even one week following the initial assembly (Figure S36). Similar supramolecular assemblies have been observed with gemini amphiphiles that have interparticle associations stabilized by interactions between the hydrophilic interfaces.33,34 We hypothesize that, analogously, electrostatic interactions between the peptides in the cylinder corona stabilize the supramolecular architecture. Supporting this hypothesis, only spherical particles are observed when on BAs-XTEN2 was assembled with an additional 100 mM NaCl that provides charge screening (Figure S36).

After identifying three morphologies formed by PPA assemblies, we sought to quantify differences between the populations formed by each PPA. To measure the diameters of the particles, we developed a semi-automated image

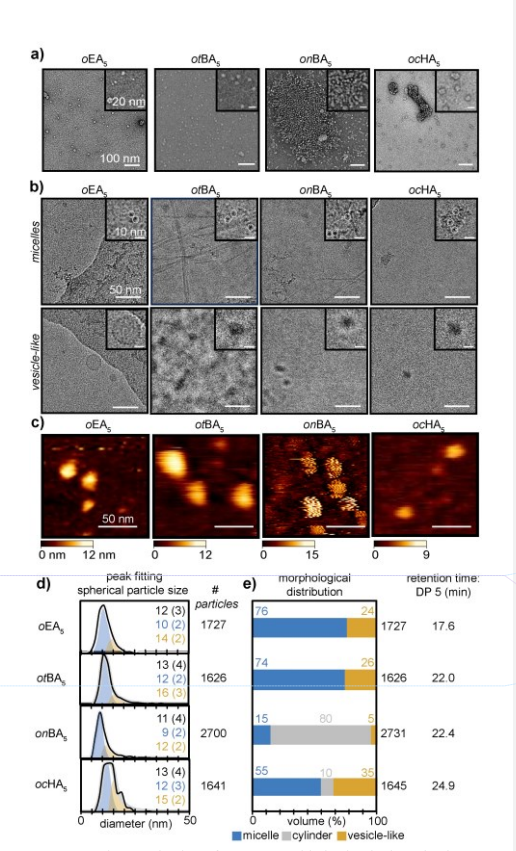


Figure 2: Characterization of PPAs assembled using bath sonication (a) Representative TEM images for PPAs (left to right): oligo(ethyl acrylate) (oEA₅), oligo(n-butyl acrylate) (onBA₅), oligo(tert-butyl acrylate) (otBAs), and oligo(cyclohexyl acrylate) (ocHAs); scale bars represent 100 nm. Inset images show higher magnification images of nanoparticles; Scale bar represents 20 nm. b) Representative cryo-EM images capturing micelles (top row) and vesicle-like particles (bottom row). Scale bar represents 50 nm. Inset images show higher magnification images of micelles nd vesicle-like nanoparticles respectively; Scale bare represents 10 nm. (c) Representative in-solution AFM images for PPAs; scale bars represent 50 nm. Bars located underneath each AFM image reflect the relative height of the particles from the mica surface. (d) Peak fitting applied to the histograms of spherical particle diameters measured from NS-TEM images to estimate the population and size for micelles and vesicle-like particles. Black = raw data, blue = Gaussian-fit micelle distribution, yellow = lognormal-fit vesicle-like distribution, and gray = sum of both fits. Average (standard deviation) for total spherical particles (black), micelles (blue) and vesicle-like particles (vellow) diameters are in the top right corner of each histogram. (e) Morphological distributions for each amphiphile based on fitting of histograms and pixel areas for each morphology; blue = micelle, yellow = vesicle-like particles, and gray = cylinders.

quantification protocol. Briefly, NS-TEM images were preprocessed using ImageJ to generate image masks, followed by extraction of the particle diameters using a MATLAB script (Script_Polymer_Analysis)³⁵ (Scheme S2). As Cryo-EM confirmed the presence of both micelles and vesicle-like particles (Figure 2b), we assumed that both particle types **Commented [AK1]:** Did they say why they didn't see it? My in stinct is to call out that this is a similar size scale

Commented [BA2R1]: They did not:/ but I do like the idea of calling out the sizes!

Commented [AK3]: See what you think about my edits here

would be reflected in their spherical particle measurements from TEM images. To determine the average diameters of the micelle and vesicle-like particles for each PPA assembly, the full spherical particle population was fit to the sum of a Gaussian fit for the micelle population and lognormal fit for the vesicle-like population, assuming a small overlap between both fits. (Figure 2d). ^{21,36-39} As in our previous study, we were able to identify two peaks in each PPA's spherical particle histogram, with the combined fits of both peaks aligning with the raw data. ⁴⁰ The peak centers of both fits were used to calculate the average micelle and vesicle-like particle diameters respectively, along with the standard deviation of each fit based on their full-width at half max to reflect the width of the distribution.

Average nanoparticle diameters were similar across the amphiphile assemblies, which we attribute to the uniform average PPA length (Figure 1d); however, small differences were observed in the micelle and vesicle-like diameters within the series. Both oEA5-XTEN2 and onBA5-XTEN2 have smaller micelle diameters (10 nm and 9 nm, respectively) than otBA5-XTEN2 and ocHA5-XTEN2 (12 nm; Figure 2d). The onBA5 and otBA5 tails are isomers, both containing four carbons in the pendent chain, indicating that differences in particle size are influenced by the architecture. Bulkier side chains have been observed to exhibit restricted interdigitation, diminishing their capacity to interact with adjacent chains during assembly and resulting in the formation of larger nanoparticles.41 Extending this hypothesis to otBA5-XTEN2 and ocHA5-XTEN2, the bulky side-chains hinder efficient packing. Leveraging variations in the bulkiness of pendent sidechains provides a strategic approach to fine-tuning nanoparticle size without necessitating modifications to the peptide composition of the PPA.

To quantify the ratio of micelles, vesicle-like particles, and cylinders in each PPA assembly, the pixel area of each morphology was calculated from the NS-TEM images and compared to amphiphile hydrophobicity as approximated using the HPLC retention time of comparable oligomers (DPtail=5; Figure 2e). Analogous to block copolymers, 21,42 more hydrophobic amphiphiles (e.g., ocHA5-XTEN2) form a larger population of vesicle-like particles, an intermediate hydrophobicity leads to cylindrical particle formation (e.g., onBA5-XTEN2), and predominantly micelles are formed by the least hydrophobic amphiphiles, oEA5-XTEN2 and otBA5-XTEN2 (Figure 2e). Despite the difference in hydrophobicity between otBA5 and oEA5, their respective PPAs form similar morphological distributions. We hypothesize that the formation of assemblies with lower curvature (i.e., cylindrical assemblies and vesicle-like particles) is stifled for otBA5-XTEN2 due to limited interdigitation. 43,44 Consequently, the hydrophobicity of the amphiphile and pendent group composition can be orthogonal tools to tune the morphologies of PPA nanoparticles.

Motivated by the block-copolymer-like behavior exhibited by the PPAs, we sought to determine whether kinetically "frozen" morphologies, typical of amphiphilic block copolymers, 8.24 could be accessed with PPAs. This phenomenon occurs when unimer exchange (i.e., exchange of a single amphiphile between assemblies) is limited due to high interfacial tension between the amphiphile and the solvent. To

probe this phenomenon, we selected an additional protocol for amphiphile assembly, thermal annealing, and monitored changes in the assembled morphologies. ^{24,45,46} Thermal annealing (80 °C, 300 rpm, 1 h followed by cooling to rt) of each PPA in buffer conditions consistent with the sonication-driven assembly similarly yielded multiple particle types observed by NS-TEM and cryo-EM (Figures 3a and S37-S43). In contrast to the sonication-driven assembly, these PPA assemblies had more uniform micelle (8-10 nm) and vesicle-like particle diameters (12-14 nm; Figure 3b). While oEA5-XTEN2 and onBA5-XTEN2 maintain consistent particle diameters between assembly methods, thermally annealing otBA5-XTEN2 and ocHA5-XTEN2 reduced micelle and vesicle-like diameters compared to sonication-induced assembly, suggesting kinetically trapped assemblies. ⁸ As

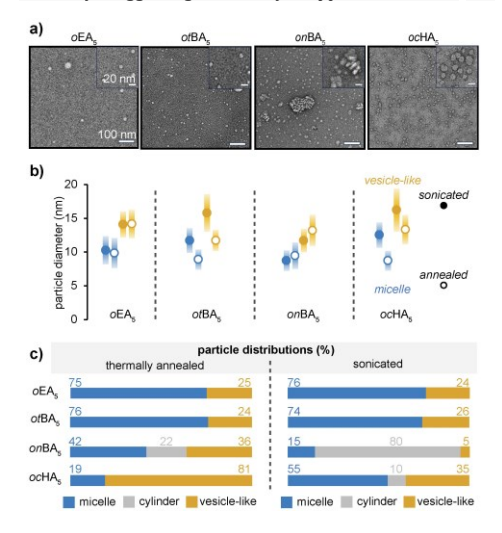


Figure 3: Analysis of negatively stained TEM images of the PPAs assembled by thermal annealing (80 °C, 300 rpm, 1 h, cool rt on). (a) Representative TEM images for each of the four amphiphiles composed of the XTEN2 peptide and each hydrophobic tail; scale bars represent 100 nm. Inset images show higher magnification images of nanoparticles; Scale bar represents 20 nm. (b) Plot comparing the micelle and vesicle-like particle diameters (standard deviation) for each amphiphile between thermal annealing and sonication-based assembling using fitted histograms generated by measured spherical particle diameters from NS-TEM images. (c) Plot comparing the morphological distributions for each amphiphile for thermal annealing and sonication-based assembly. Blue = micelle, gray = cylinder, and yellow = vesicle-like particles throughout.

both of these materials have bulky side chains, we hypothesize that the increase in temperature using thermal annealing allows increased exchange of amphiphile chains, leading to increased interdigitation of their hydrophobic membranes. $^{47.48}$ As $o\mathrm{EA_5}\text{-XTEN2}$ and $on\mathrm{BA_5}\text{-XTEN2}$ do not change in diameter for micelles or vesicle-like nanoparticles, their cores are likely well packed using either bath sonication or thermal annealing induced assemblies.

In addition to decreasing spherical particle sizes, there is also a change in the morphological distributions; the

population of cylindrical bundles decreases for both onBA₅-XTEN2 and ocHA₅-XTEN2 (Figure 3c). Of note, ocHA₅-XTEN2 forms primarily vesicle-like nanoparticles when assembled with thermal annealing; similarly, the population of onBA₅-XTEN2 shifts towards vesicle-like nanoparticles. However, oEA₅-XTEN2 and otBA₅-XTEN2 have comparable distributions with both assembly methods. As both experimental and computational studies have suggested that vesicle formation can proceed through cylindrical micelle intermediates, ⁴⁹⁻⁵² we hypothesize that thermal annealing uniquely allows the transition from a cylindrical to a vesicle-like morphology for these PPAs through an increased

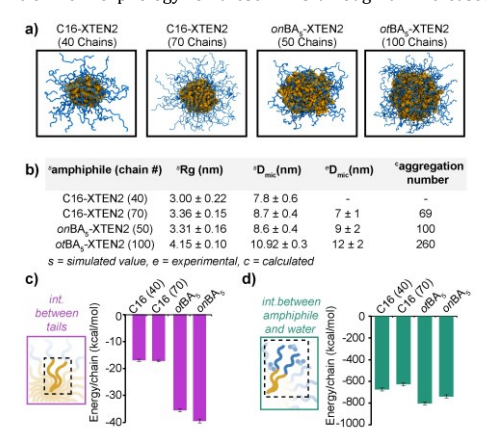


Figure 4. All-atom molecular dynamics simulations of selected amphiphiles. (a) Final snapshots of assembled micelles for C16-XTEN2 (40 chains and 70 chains), onBA₃-XTEN2 (50 chains), and onBA₃-XTEN2 (100 chains) after simulation convergence. Water and salt atoms are removed for visualization. (b) Comparison of simulation obtained parameters (radius of gyration, "R_{glmicelis}) and micelle diameter, 'D_{mic}) and calculated aggregation number calculated using microscopy images. (c) Non-bonded interaction energy calculated between tails averaged per chain. (d) Non-bonded interaction energy calculated between amphiphiles and water averaged per chain. For c and d, data is averaged over two simulations for each amphiphile. The error bars represent the standard deviation from multiple frames from two simulations.

rate of amphiphile exchange. This change in morphology indicates that \emph{on} BA₅-XTEN2 also forms kinetically trapped assemblies.⁸

Though otBA5-XTEN2, onBA5-XTEN2, and ocHA5-XTEN2 form kinetically trapped assemblies,⁸ we observed no change in the morphological distribution or nanoparticle sizes of oEA5-XTEN2 between the assembly protocols (Figure 3b-c). While this does not confirm that it reaches a thermodynamic equilibrium, it does suggest that oEA5-XTEN2 has a lower interfacial tension and thus higher rate of unimer exchange than the other PPAs.¹⁶ To further probe this observation, we monitored the particle sizes of oEA5-XTEN2 and otBA5-XTEN2 following incubation at room temperature for one week after the initial assembly, as no shift in morphology was observed for either amphiphile using different assembly mechanisms (Figure 3c). After one week, OEA5-XTEN2 maintained uniform particle sizes as observed by NS-TEM (Figure S44), indicative of rapid unimer

equilibrium and a long-lived morphology. ¹⁶ In contrast, otBA₅-XTEN2 nanoparticles displayed aggregation after one week (Figure S45), which is common for materials with limited exchange as the particles collide over time. ⁸

To investigate the complexities of atomic-level processes driving the PPA assembly dynamics and final structure of micelles, all-atomistic molecular dynamics (AMD) was used. These simulations contained up to 100 PPAs with over 1 million atoms in explicit solvent, with the longest simulation conducted for 500 ns of simulation time. Due to the computational expense of such simulations, only the isomeric amphiphiles, onBA5-XTEN2 and otBA5-XTEN2, were selected. Additionally, a lipid control was also screened, C16-XTEN2, as lipid tails are well-studied experimentally and computationally.53-55 The simulations were initiated from a loosely prearranged spherical micelle shape to decrease the required simulation time (Figure S46-S49). All simulations were run in duplicate to provide confidence in calculated parameters. The choice of a total number of simulated amphiphile chains was guided by the aggregation number estimated from experimental characterization of the micelle size and simulated amphiphile volume but was capped at 100 chains due to computational cost (Table S1).

For comparison of acrylate oligomers to a lipid control, the C16-XTEN2 amphiphile was experimentally synthesized by coupling palmitic acid to the N-terminus of an XTEN2 sequence lacking the N-terminal cysteine residue and purification proceeded with semi-preparative HPLC (Figure S50). Self-assembly via thermal annealing of C16-XTEN2 showed micelle formation by both NS-TEM and cryo-EM (Figures S51-S53). To ensure that the number of simulated chains minimally impacted the formation of a micelle and the resultant structure, the C16-XTEN2 amphiphile, containing the fewest atoms, was simulated using 70 chains, corresponding to approximately the experimental aggregation number, and a computationally less expensive 40 chains. The snapshots obtained from the simulations illustrate the final structure of the micelles (Figure 4a), and the simulated micelle diameters (sDmic) were similar to the experimentally derived values (eDmic; Figures 4b, Table S2). The sDmic was calculated using the simulation obtained average radius of gyration of the micelle (sRg(micelle)) with the following equation:56

$$^{s}D_{mic} = 2\sqrt{\frac{5}{3}} \, ^{s}R_{g(micelle)}$$

Notably, comparable values were obtained for the two C16-XTEN2 simulations, suggesting tolerance in the number of chains used in the simulation.

To understand key interactions dictating micellar structure, non-bonded interaction energies between amphiphilic chains or the surrounding environment were computed from the simulations, averaging across the two simulations (Figure S53-S54). Interactions between the hydrophobic tails within the micelle core correlate with the experimentally observed hydrophobicity calculated using the amphiphile retention time: the weakest interactions per chain were observed for C16, followed by otBAs, then onBAs (Figures 4c and 2e, C16-XTEN2 retention time = 19.7 min). Additionally, the two simulations of C16-XTEN2 (40 and 70

chains) provided consistent energetic values per chain, suggesting that the chemical structure of the tail is more important than the number of chains used in the simulation. Finally, the strength of the tail-tail interactions further supports our hypothesis that $onBA_5$ containing amphiphiles can more easily access lower curvature morphologies with more self-interactions than $otBA_5$.

To probe the relationship between tail composition and interfacial tension, we calculated the non-bonded interaction energy between water and the selected amphiphiles, averaging over the two simulations (Figures 4d, S54). Notably, the C16 amphiphile (40 and 70 chains) exhibits the lowest non-bonded interaction energy with water, while otBA5-XTEN2 has a higher energy per-chain as compared to onBA5-XTEN2. This indicates a higher interfacial tension for the PPAs as compared to C16-XTEN2, which aligns with the observation of kinetically "frozen" assemblies for otBA5-XTEN2 and onBA5-XTEN2. Further, an increased volume of the hydrophobic block has been shown to increase amphiphile interfacial tension ^{23,57} which is consistent with otBA5-XTEN2 having a higher energy than onBA5-XTEN2 (Table S3).

As water molecules play a significant role in micelle formation, we analyzed the water molecules present within the assembled structures. Both C16-XTEN2 micelles have a dehydrated core with water present only in the outer shell (Figure 5). Interestingly, onBA5-XTEN2and otBA5-XTEN2 formed both dehydrated and hydrated cores. Although the hydration of hydrophobic tails is energetically unfavorable, we hypothesize that the presence of hydrophilic ester groups in the oligomeric tail backbone can enable the penetration of water molecules inside the hydrophobic core.⁵⁸

Since the total number of hydrophilic groups within each otBA5 and onBA5 tail is the same, we expected a similar number of water molecules inside each core. However, we observed a higher water density inside the core of otBA5-XTEN2 as compared to onBA5-XTEN2 (Figure 5b, S56). Notably, the water molecules inside the core of both on BA5-XTEN2 and otBA5-XTEN2 are dynamic, as visualized over the last 14 ns of the simulations (Video S1, S57). We have previously observed that a small structural change in the conformation of biopolymers can lead to different amounts of water trapped inside coacervates.⁵⁹ Hence, despite having the same number of carbon atoms in the side chain, we hypothesize the bulkiness of the otBA side chain prohibits high density packing of amphiphile chains, enabling greater accommodation of water molecules during the self-assembly process. The presence of water-rich domain inside the oligomer cores supports their ability to form vesicle-like materials,30-32 contributing to the complex landscape of morphologies formed by the PPAs.

Conclusion

Through this systematic study of diblock oligomeric peptide-polymer amphiphile (PPA) assemblies, we have elucidated the impact of monomer composition on nanoparticle morphology and dynamics. This work demonstrates that increasing oligomer block hydrophobicity, while maintaining block length, results in predictable morphological trends. Additionally, higher hydrophobic volumes lead to

kinetically trapped nanoparticles due to an elevated interfacial tension with water. This affords orthogonal tunability of nanoparticle size and morphology through different self-assembly methods, including bath sonication and thermal annealing. Furthermore, all-atomistic molecular dynamics simulations revealed correlations between non-bonded interaction energies and experimental characterization of hy-

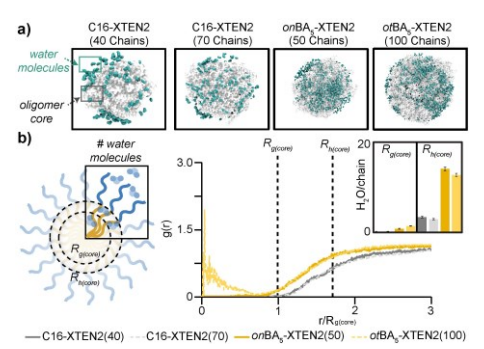


Figure 5: Characterization of water inside the hydrophobic core of peptide amphiphiles. (a) Snapshots of water molecules (teal) within the first water shell (3.4 Å) of the amphiphile hydrated cores (white) [left to right: C16-XTEN2 (40 chains and 70 chains), onBA₃-XTEN2 (50 chains), and otBA₃-XTEN2 (100 chains)]. (b) (Left) Schematic of the radius of gyration of core (R_{8[cone]}) and radius of hydration of core (R_{8[cone]}) and radius of hydration of core (R_{4[cone]}). (Right) Plot of the radial distribution function of water, distance (r) normalized by the radius of gyration of core, for C16-XTEN2 (40 chains; solid dark gray), C16-XTEN2 (70 chains; light dashed gray), onBA₃-XTEN2 (50 chains; solid dark yellow), and orBA₃-XTEN2 (100 chains; dashed light yellow). Black dashed vertical lines illustrate R_{8[cone]} and R_{8[cone]}. Inset bar plot shows the number of waters per amphiphile chain in both the R_{8[cone]} and R_{8[cone]}. Data is averaged over two simulations for amphiphile. The error bars represent the standard deviation from multiple frames from two simulations.

drophobicity, in addition to offering a valuable tool for characterizing interfacial tension of amphiphiles. Moreover, these simulations revealed variable hydration of the hydrophobic cores, highlighting the significance of subtle structural variations in tail composition. Overall, these findings highlight the intricate tunability PPAs offer for controlled nanoparticle formation, providing a modular platform for the rational design of bioinspired functional assemblies.

Future research with PPAs is poised to continue to integrate the synthetic versatility of polymers with the biomimetic capabilities of peptides to better emulate and expand on natural functionality. Fine-tuning the molecular weight dispersity could enable access to specific morphologies mimicking natural organelles or biophysical properties such as controlled membrane fluidity, which is critical for drug delivery. Further, the use of functional peptides with requisite secondary structure can allow biomimetic functionality such as metal sequestration and catalysis. PPAs can be further incorporated into biotechnologies and biomedicines by utilizing antimicrobial peptides for targeted cell lysis or assembling into stable nanostructures for energy storage. Understanding how peptide and polymer composition influence hierarchical assemblies will allow biohybrid materials to better emulate biological functionality seen in protein complexes, bringing synthetic materials closer to natural efficacy.

ASSOCIATED CONTENT

Supporting Information.

Supporting information contains the experimental details, synthetic procedures, image analysis procedure, modeling simulation parameters, and supplemental figures and tables NMR, SEC, microscopy images for: NS-TEM, Cryo-EM, and AFM, and other characterization.

The Supporting Information is available free of charge on the ACS Publications website.

ACKNOWLEDGMENT

This material is based upon experimental work (A.S.K.) supported by the Air Force Office of Scientific Research under Award Number FA9550-20-1-0172 and computational work (Y.G.Y.) supported through the National Science Foundation Macromolecular, Supramolecular, and Nanochemistry Program under Award Number CHE-2108818. B.P.A. thanks the UNC Program in Molecular and Cellular Biophysics (MCBP) National Institutes of Health (NIH) training fellowship (T32GM008570). AFM characterization was supported by the National Institute of General Medical Sciences (NIGMS) (R35 GM127151). TEM was performed in part at the Chapel Hill Analytical and Nanofabrication Laboratory, CHANL, a member of the North Carolina Research Triangle Nanotechnology Network, RTNN, which is supported by the National Science Foundation, Grant ECCS-1542015, as part of the National Nanotechnology Coordinated Infrastructure, NNCI, We acknowledge Dr. Joshua Strauss of the UNC CryoTEM Core Facility and Dr. Kedar Sharma for technical assistance in this project, as well as Will Simke for guidance in the development of the image analysis tool.

ABBREVIATIONS

PAs, peptide amphiphiles, oEA, oligo(ethyl acrylate), otBA, oligo(tert-butyl acrylate), onBA, oligo(n-butyl acrylate), and ocHA, oligo(cyclohexyl acrylate), DP, degree of polymerization, Mn, number average molecular weight, Mw, weight average molecular weight, Ð, dispersity, PPA, peptide-polymer amphiphile, HPLC, reversed-phase high performance liquid chromatography, LC-MS, liquid chromatography-mass spectrometry, HEPES, 4-(2-hydroxyethyl)-1-piperazineethanesulfonic acid, TCEP, tris(2-carboxylethyl)phosphine, DMF, dimethyl formamide, oEA5-XTEN2, oligo(ethyl acrylate, DP =5)-XTEN2, onBA5-XTEN2, oligo(n-butyl acrylate, DP =5)-XTEN2, otBA5-XTEN2, oligo(tert-butyl acrylate, DP =5)-XTEN2, ocHA5-XTEN2, oligo(cyclohexyl acrylate, DP = 5)-XTEN2, NS-TEM, negative-stain transmission electron microscopy, cryo-EM, cryogenic electron microscopy, AFM, atomic force microscopy, C16-XTEN2, palmitic acid-XTEN2, sRg(micelle), simulated radius of gyration for micelle, Rh(core) radius of hydration for micelle core, (Rg(core)), radius of gyration of micelle core, sDmic, simulated micelle diameter, eDmic, experimentally calculated micelle diameter, AMD, allatomistic molecular dynamics.

REFERENCES

- Dasgupta, A.; Das, D. Designer Peptide Amphiphiles: Self-Assembly to Applications. *Langmuir* 2019, 35 (33), 10704–10724. https://doi.org/10.1021/acs.langmuir.9b0183
- (2) Cui, H.; Webber, M. J.; Stupp, S. I. Self-Assembly of Peptide Amphiphiles: From Molecules to Nanostructures to Biomaterials. *Biopolymers* 2010, 94 (1), 1–18. https://doi.org/10.1002/bip.21328.
- (3) Pramanik, B.; Ahmed, S.; Singha, N.; Das, D. Self-Assembly Assisted Tandem Sensing of Pd2+ and CN- by a Perylenediimide-Peptide Conjugate. *ChemistrySelect* 2017, 2, 10061–10066. https://doi.org/10.1002/slct.201701849.
- (4) Ahmed, S.; Pramanik, B.; Sankar, K. A.; Srivastava, A.; Singha, N.; Dowari, P.; Srivastava, A.; Mohanta, K.; Debnath, A.; Das, D. Solvent Assisted Tuning of Morphology of a Peptide-Perylenediimide Conjugate: Helical Fibers to Nano-Rings and Their Differential Semiconductivity. Sci. Rep. 2017, 7 (1), 9485.
- (5) Ahmed, S.; Amba Sankar, K. N.; Pramanik, B.; Mohanta, K.; Das, D. Solvent Directed Morphogenesis and Electrical Properties of a Peptide–Perylenediimide Conjugate. *Langmuir* 2018, 34 (28), 8355–8364. https://doi.org/10.1021/acs.langmuir.8b0175 0.
- (6) Mitchison, T. J.; Biol, J. C.; Kelleher, J. F.; Atkinson, S. J.; Pollard, T. D.; Biol, J. C.; Hartgerink, J. D.; Beniash, E.; Stupp, S. I. Self-Assembly and Mineralization of Peptide-Amphiphile Nanofibers. 2001, 294 (November), 1684–1689.
- (7) Dasgupta, A. Exploring Architectures at the Nanoscale: The Interplay between Hydrophobic Twin Lipid Chains and Head Groups of Designer Peptide Amphiphiles in the Self-Assembly Process and Application. Soft Matter 2016, 12 (19), 4352–4360. https://doi.org/10.1039/c6sm00147e.
- (8) Nicolai, T.; Colombani, O.; Chassenieux, C. Dynamic Polymeric Micelles versus Frozen Nanoparticles Formed by Block Copolymers. *Soft Matter* **2010**, *6* (14),

- 3111–3118. https://doi.org/10.1039/b925666k.
- (9) Barbee, M. H.; Wright, Z. M.; Allen, B. P.; Taylor, H. F.; Patteson, E. F.; Knight, A. S. Protein-Mimetic Self-Assembly with Synthetic Macromolecules. 2021. https://doi.org/10.1021/acs.macromol.0c028 26
- (10) Trent, A.; Marullo, R.; Lin, B.; Black, M.; Tirrell, M. Structural Properties of Soluble Peptide Amphiphile Micelles. *Soft Matter* 2011, 7 (20), 9572–9582. https://doi.org/10.1039/C1SM05862B.
- (11) Li, Q.; Wang, Y.; Zhang, G.; Su, R.; Qi, W. Biomimetic Mineralization Based on Self-Assembling Peptides. *Chem. Soc. Rev.* 2023, 52 (5), 1549–1590. https://doi.org/10.1039/D2CS00725H.
- (12) Hendricks, M. P.; Sato, K.; Palmer, L. C.; Stupp, S. I. Supramolecular Assembly of Peptide Amphiphiles. *Acc. Chem. Res.* 2017, 50 (10), 2440–2448. https://doi.org/10.1021/acs.accounts.7b0029 7.
- (13) Mardilovich, A.; Craig, J. A.; McCammon, M. Q.; Garg, A.; Kokkoli, E. Design of a Novel Fibronectin-Mimetic Peptide–Amphiphile for Functionalized Biomaterials. *Langmuir* 2006, 22 (7), 3259–3264. https://doi.org/10.1021/la052756n.
- (14) Kokkoli, E.; Mardilovich, A.; Wedekind, A.; Rexeisen, E. L.; Garg, A.; Craig, J. A. Self-Assembly and Applications of Biomimetic and Bioactive Peptide-Amphiphiles. Soft Matter 2006, 2 (12), 1015–1024. https://doi.org/10.1039/b608929a.
- (15) Shu, J. Y.; Panganiban, B.; Xu, T. Peptide-Polymer Conjugates: From Fundamental Science to Application. *Annu. Rev. Phys. Chem.* 2013, 64 (1), 631–657. https://doi.org/10.1146/annurev-physchem-040412-110108.
- (16) Wright, D. B.; Ramírez-Hernández, A.; Touve, M. A.; Carlini, A. S.; Thompson, M. P.; Patterson, J. P.; De Pablo, J. J.; Gianneschi, N. C. Enzyme-Induced Kinetic Control of Peptide-Polymer Micelle Morphology. ACS Macro Lett. 2019, 8 (6), 676–681.

- https://doi.org/10.1021/acsmacrolett.8b00887.
- (17) Callmann, C. E.; Thompson, M. P.; Gianneschi, N. C. Poly (Peptide): Synthesis, Structure, and Function of Peptide–Polymer Amphiphiles and Protein-like Polymers. Acc. Chem. Res. 2020, 53 (2), 400–413.
- (18) Doncom, K. E. B.; Blackman, L. D.; Wright, D. B.; Gibson, M. I.; O'Reilly, R. K. Dispersity Effects in Polymer Self-Assemblies: A Matter of Hierarchical Control. Chem. Soc. Rev. 2017, 46 (14), 4119–4134.
- (19) Jiang, Y.; Chen, T.; Ye, F.; Liang, H.; Shi, A. C. Effect of Polydispersity on the Formation of Vesicles from Amphiphilic Diblock Copolymers. *Macromolecules* 2005, 38 (15), 6710–6717. https://doi.org/10.1021/ma050424j.
- (20) Blanazs, A.; Armes, S. P.; Ryan, A. J. Self-assembled Block Copolymer Aggregates: From Micelles to Vesicles and Their Biological Applications. *Macromol. Rapid Commun.* 2009, 30 (4-5), 267–277.
- (21) Allen, B. P.; Wright, Z. M.; Taylor, H. F.; Oweida, T. J.; Kader-Pinky, S.; Patteson, E. F.; Bucci, K. M.; Cox, C. A.; Senthilvel, A. S.; Yingling, Y. G.; Knight, A. S. Mapping the Morphological Landscape of Oligomeric Di-block Peptide–Polymer Amphiphiles. *Angew. Chem. Int. Ed.* 2022. https://doi.org/10.1002/anie.202115547.
- (22) Kranenburg, M.; Venturoli, M.; Smit, B. Phase Behavior and Induced Interdigitation in Bilayers Studied with Dissipative Particle Dynamics. J. Phys. Chem. B 2003, 107 (41), 11491–11501.
- (23) Creutz, S.; van Stam, J.; Antoun, S.; De Schryver, F. C.; Jérôme, R. Exchange of Polymer Molecules between Block Copolymer Micelles Studied by Emission Spectroscopy. A Method for the Quantification of Unimer Exchange Rates. Macromolecules 1997, 30 (14), 4078–4083.
- (24) Murphy, R. P.; Kelley, E. G.; Rogers, S. A.; Sullivan, M. O.; Epps III, T. H. Unlocking Chain Exchange in Highly Amphiphilic Block Polymer Micellar Systems: Influence of Agitation. ACS Macro Lett. 2014, 3 (11), 1106–1111.

- (25) Matyjaszewski, K. Atom Transfer Radical Polymerization (ATRP): Current Status and Future Perspectives. *Macromolecules* 2012, 45 (10), 4015–4039. https://doi.org/10.1021/ma3001719.
- (26) Schellenberger, V.; Wang, C. W.; Geething, N. C.; Spink, B. J.; Campbell, A.; To, W.; Scholle, M. D.; Yin, Y.; Yao, Y.; Bogin, O.; Cleland, J. L.; Silverman, J.; Stemmer, W. P. C. A Recombinant Polypeptide Extends the in Vivo Half-Life of Peptides and Proteins in a Tunable Manner. *Nat. Biotechnol.* 2009, 27 (12), 1186–1190. https://doi.org/10.1038/nbt.1588.
- (27) Podust, V. N.; Balan, S.; Sim, B. C.; Coyle, M. P.; Ernst, U.; Peters, R. T.; Schellenberger, V. Extension of in Vivo Half-Life of Biologically Active Molecules by XTEN Protein Polymers. *J. Controlled Release* 2016, 240, 52–66. https://doi.org/10.1016/j.jconrel.2015.10.03 8.
- (28) Murgasova, R.; Hercules, D. M. Polymer Characterization by Combining Liquid Chromatography with MALDI and ESI Mass Spectrometry. *Anal. Bioanal. Chem.* 2002, 373 (6), 481–489. https://doi.org/10.1007/s00216-002-1332-9.
- (29) Piogé, S.; Fontaine, L.; Gaillard, C.; Nicol, E.; Pascual, S. Self-Assembling Properties of Well-Defined Poly(Ethylene Oxide)- b-Poly(Ethyl Acrylate) Diblock Copolymers. *Macromolecules* 2009, 42 (12), 4262–4272. https://doi.org/10.1021/ma802705b.
- (30) Xiao, M.; Xia, G.-J.; Wang, R.; Xie, D. Controlling the Self-Assembly Pathways of Amphiphilic Block Copolymers into Vesicles. Soft Matter 2012, 8, 7865–7874. https://doi.org/10.1039/C2SM25281C.
- (31) He, X.; Schmid, F. Dynamics of Spontaneous Vesicle Formation in Dilute Solutions of Amphiphilic Diblock Copolymers. *Macromolecules* 2006, 39 (7), 2654–2662. https://doi.org/10.1021/ma052536g.
- (32) Baoukina, S.; Monticelli, L.; Risselada, H. J.; Marrink, S. J.; Tieleman, D. P. The Molecular Mechanism of Lipid Monolayer Collapse. *Proc. Natl. Acad. Sci.* 2008, 105

- (31), 10803–10808. https://doi.org/10.1073/pnas.0711563105.
- (33) Chen, H.; Chen, J.; Wan, D.; Zhang, H.; Mao, C.; Wang, R. Self-assembly of Gemini Amphiphiles with Symmetric Tails in Selective Solvent. *Polym. Int.* 2022, 71 (9), 1082–1089.
- (34) Limouzin-Morel, C.; Dutertre, F.; Moussa, W.; Gaillard, C.; Iliopoulos, I.; Bendejacq, D.; Nicolaï, T.; Chassenieux, C. One and Two Dimensional Self-Assembly of Comblike Amphiphilic Copolyelectrolytes in Aqueous Solution. Soft Matter 2013, 9 (37), 8931–8937.
- (35) Https://Github.Com/UNC-Knight-Lab/Particle-Counting.
- (36) Nelson, P. H.; Rutledge, G. C.; Hatton, T. A. On the Size and Shape of Self-Assembled Micelles. *J. Chem. Phys.* 1997, 107 (24), 10777–10781. https://doi.org/10.1063/1.474193.
- (37) Bug, A. L. R.; Cates, M. E.; Safran, S. A.; Witten, T. A. Theory of Size Distribution of Associating Polymer Aggregates. I. Spherical Aggregates. J. Chem. Phys. 1987, 87 (3), 1824–1833. https://doi.org/10.1063/1.453195.
- (38) Chécot, F.; Brûlet, A.; Oberdisse, J.; Gnanou, Y.; Mondain-Monval, O.; Lecommandoux, S. Structure of Polypeptide-Based Diblock Copolymers in Solution: Stimuli-Responsive Vesicles and Micelles. *Langmuir* **2005**, *21* (10), 4308– 4315. https://doi.org/10.1021/la0468500.
- (39) Song, N. W.; Park, K. M.; Lee, I. H.; Huh, H. Uncertainty Estimation of Nanoparticle Size Distribution from a Finite Number of Data Obtained by Microscopic Analysis. *Metrologia* 2009, 46 (5), 480–488. https://doi.org/10.1088/0026-1394/46/5/012.
- (40) Allen, B. P.; Wright, Z. M.; Taylor, H. F.; Oweida, T. J.; Kader-Pinky, S.; Patteson, E. F.; Bucci, K. M.; Cox, C. A.; Senthilvel, A. S.; Yingling, Y. G.; Knight, A. S. Mapping the Morphological Landscape of Oligomeric Di-block Peptide-Polymer Amphiphiles**. *Angew. Chem. Int. Ed.* 2022, 61 (14), e202115547. https://doi.org/10.1002/anie.202115547.

- (41) Mei, J.; Bao, Z. Side Chain Engineering in Solution-Processable Conjugated Polymers. *Chem. Mater.* **2014**, *26* (1), 604–615.
- (42) Foster, J. C.; Akar, I.; Grocott, M. C.; Pearce, A. K.; Mathers, R. T.; O'Reilly, R. K. 100th Anniversary of Macromolecular Science Viewpoint: The Role of Hydrophobicity in Polymer Phenomena. ACS Macro Lett. 2020, 9 (11), 1700–1707.
- (43) Razzell-Hollis, J.; Fleischli, F.; Jahnke, A. A.; Stingelin, N.; Seferos, D. S.; Kim, J.-S. Effects of Side-Chain Length and Shape on Polytellurophene Molecular Order and Blend Morphology. J. Phys. Chem. C 2017, 121 (4), 2088–2098.
- (44) Balakrishnan, K.; Datar, A.; Naddo, T.; Huang, J.; Oitker, R.; Yen, M.; Zhao, J.; Zang, L. Effect of Side-Chain Substituents on Self-Assembly of Perylene Diimide Molecules: Morphology Control. J. Am. Chem. Soc. 2006, 128 (22), 7390–7398.
- (45) Foster, J. C.; Varlas, S.; Couturaud, B.; Jones, J. R.; Keogh, R.; Mathers, R. T.; O'Reilly, R. K. Predicting Monomers for Use in Polymerization-Induced Self-Assembly. *Angew. Chem. Int. Ed.* 2018, 57 (48), 15733–15737.
- (46) Schroeder, A.; Kost, J.; Barenholz, Y. Ultrasound, Liposomes, and Drug Delivery: Principles for Using Ultrasound to Control the Release of Drugs from Liposomes. Chem. Phys. Lipids 2009, 162 (1–2), 1–16.
- (47) Davidson, E. C.; Segalman, R. A. Thermal Control of Confined Crystallization within P3EHT Block Copolymer Microdomains. *Macromolecules* 2017, 50 (20), 8097–8105. https://doi.org/10.1021/acs.macromol.7b016 16.
- (48) Gupta, S.; Lodge, T. P. Effect of Changing Interfacial Tension on Fragmentation Kinetics of Block Copolymer Micelles. *Macromolecules* 2023, 56 (5), 2137–2148. https://doi.org/10.1021/acs.macromol.2c021 58.
- (49) Egelhaaf, S. U.; Schurtenberger, P. Micelleto-Vesicle Transition: A Time-Resolved Structural Study. *Phys. Rev. Lett.* **1999**, 82 (13), 2804.
- (50) Figg, C. A.; Carmean, R. N.; Bentz, K. C.; Mukherjee, S.; Savin, D. A.; Sumerlin, B. S.

- Tuning Hydrophobicity to Program Block Copolymer Assemblies from the inside Out. *Macromolecules* **2017**, *50* (3), 935–943.
- (51) Chen, L.; Shen, H.; Eisenberg, A. Kinetics and Mechanism of the Rod-to-Vesicle Transition of Block Copolymer Aggregates in Dilute Solution. *J. Phys. Chem. B* 1999, 103 (44), 9488–9497. https://doi.org/10.1021/jp9913665.
- (52) Zhang, L.; Sevink, A.; Schmid, F. Hybrid Lattice Boltzmann/Dynamic Self-Consistent Field Simulations of Microphase Separation and Vesicle Formation in Block Copolymer Systems. *Macromolecules* 2011, 44 (23), 9434–9447. https://doi.org/10.1021/ma2018638.
- (53) Manandhar, A.; Kang, M.; Chakraborty, K.; Tang, P. K.; Loverde, S. M. Molecular Simulations of Peptide Amphiphiles. *Org. Biomol. Chem.* 2017, *15* (38), 7993–8005. https://doi.org/10.1039/c7ob01290j.
- (54) M. Frederix, P. W. J.; Patmanidis, I.; J. Marrink, S. Molecular Simulations of Self-Assembling Bio-Inspired Supramolecular Systems and Their Connection to Experiments. *Chem. Soc. Rev.* 2018, 47 (10), 3470–3489. https://doi.org/10.1039/C8CS00040A.
- (55) McCullagh, M.; Prytkova, T.; Tonzani, S.; Winter, N. D.; Schatz, G. C. Modeling Self-Assembly Processes Driven by Nonbonded Interactions in Soft Materials. J. Phys. Chem. B 2008, 112 (34), 10388–10398. https://doi.org/10.1021/jp803192u.
- (56) Bogusz, S.; Venable, R. M.; Pastor, R. W. Molecular Dynamics Simulations of Octyl Glucoside Micelles: Structural Properties. *J. Phys. Chem. B* 2000, 104 (23), 5462– 5470. https://doi.org/10.1021/jp000159y.
- (57) Stafford, R. E.; Fanni, T.; Dennis, E. A. Interfacial Properties and Critical Micelle Concentration of Lysophospholipids. *Biochemistry* 1989, 28 (12), 5113–5120.
- (58) Menger, F.; Jerkunica, J.; Johnston, J. The Water Content of a Micelle Interior. The Fjord vs. Reef Models. J. Am. Chem. Soc. 1978, 100 (15), 4676–4678.
- (59) Li, N. K.; Xie, Y.; Yingling, Y. G. Insights into Structure and Aggregation Behavior of Elastin-like Polypeptide Coacervates: All-

Atom Molecular Dynamics Simulations. *J. Phys. Chem. B* **2021**, *125* (30), 8627–8635. https://doi.org/10.1021/acs.jpcb.1c02822.

SYNOPSIS TOC

Diblock oligomeric peptide-polymer amphiphiles (PPAs) combine sequence-defined peptides with hydrophobic oligomeric tails to facilitate multi-chain nanoparticle assembly. Herein, we describe a systematic investigation of the relationships between hydrophobic monomer composition and assembly mechanism on nanoparticle formation using experimental and computational approaches, revealing how monomer hydrophobicity and composition are independent factors that can be leveraged to tune both nanoparticle size and shape.

Now your page is set up so that figures, schemes, charts, and tables can span two columns. These must appear at the top of the page. Be sure to add another section break after the table and change it back to two columns with a spacing of 0.33 in.

Authors are required to submit a graphic entry for the Table of Contents (TOC) that, in conjunction with the manuscript title, should give the reader a representative idea of one of the following: A key structure, reaction, equation, concept, or theorem, etc., that is discussed in the manuscript. Consult the journal's Instructions for Authors for TOC graphic specifications.

Insert Table of Contents artwork here

